ACS OMEGA

Open Access

http://pubs.acs.org/journal/acsodf

Article

Alginate Cryogels for Rapid Hemostasis and Toluidine Blue-Mediated Photodynamic Inactivation of Bacteria

Xiaocheng Lin,[§] Jia Chen,[§] Yu Xia,[§] Yan Chen, Huixuan Gan, Zhongjia Liu, Quanxin Wu, Yang Zhang,* and Ning Guo*

Cite This: *ACS Omega* 2024, 9, 35845−35852

Read Online

ACCESS | Metrics & More | Article Recommendations | Supporting Information

ABSTRACT: The development of new wound dressings with fast hemostatic and bactericidal properties for prehospital care is critical. Antibacterial photodynamic therapy (aPDT) has attracted attention due to its broad-spectrum antibacterial activity and minimal bacterial resistance. However, photosensitizers used in aPDT often face issues such as poor water solubility, short-lived singlet oxygen ($^1O_2$), and limited $^1O_2$ diffusion range. In this study, sodium alginate was covalently modified with the photosensitizer toluidine blue O (TBO) and phenylboronic acid (PBA). The modified alginate was then cross-linked with Ca(II) ions and lyophilized to form a cryogel, named SA@Ca(II)@TBO@PBA (SCTP). This cryogel functions as an antibacterial photodynamic wound dressing. The chemical immobilization of TBO and PBA enhanced the cryogel's targeting ability. PBA formed reversible covalent bonds with diol groups on bacterial cell surfaces, allowing the cryogel to capture bacteria effectively and enhance aPDT. The bactericidal efficiency of the cryogel was tested through in vitro antibacterial assays, and its hemostatic properties were confirmed in vivo. The results indicate that this cryogel has excellent hemostatic and antibacterial capabilities, showing great promise as a wound dressing for clinical applications.

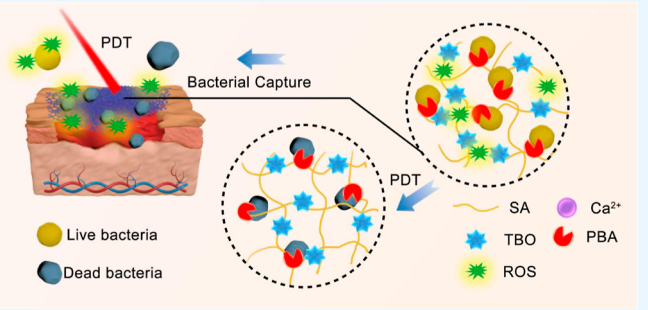

1. INTRODUCTION

Injuries to the skin often result in uncontrollable bleeding, a leading cause of trauma-related fatalities worldwide.[1] To mitigate this risk and prevent infections, effective wound dressings are essential for immediate treatment before reaching the hospital. Cryogels, among various types of wound dressings like hydrogels, hydrofibers, foams, and hydrocolloids, are particularly promising due to their high porosity and large surface area, facilitating superior fluid absorption compared to traditional dressings.[2−7] Cryogels, formed through the lyophilization of hydrogels, have shown potential in clinical trials for hemorrhage control.[7−10] Despite their efficacy, there is a growing need for novel cryogel materials that offer both rapid hemostasis and antimicrobial properties. Sodium alginate (SA) stands out as a promising material for cryogels due to its biocompatibility, low immunogenicity, and biodegradability, making it suitable for in vivo applications.[11−14] By leveraging Ca(II)-mediated ionotropic gels and freeze-drying techniques, SA-based cryogels can be easily fabricated while maintaining the three-dimensional structure of the wet gels. However, conventional SA-based cryogels often lack antimicrobial properties, underscoring the demand for functional biomaterials with enhanced bactericidal capabilities.

To address bacterial infections in wounds using cryogels, researchers have traditionally added antibiotics to create antibacterial cryogels.[15,16] However, this approach has drawbacks, including the risk of antibiotic resistance.[17,18] Eventually, it is predicted by World Health Organization that about 10 million people will die of antimicrobial resistance each by 2050.[19] To tackle this issue, nonantibiotic antibacterial methods like photothermal therapy (PTT), sonodynamic therapy, chemodynamic therapy, and photodynamic therapy (PDT) have gained attention.[20−27] PDT, in particular, is promising because it generates singlet oxygen ($^1O_2$) upon laser exposure, effectively killing bacteria without causing resistance.[28,29] Cryogel materials have porous structure. When PDT is combined with cryogel materials, the contact area between photosensitizer and oxygen can be increased. In addition, the porosity of cryogel materials can also increase the penetration distance of the laser.[30] Despite these advantages, photodynamic cryogels still face challenges, such as the short lifespan and limited spread of $^1O_2$. Thus, novel strategies are needed to enhance their effectiveness.

Received: May 20, 2024
Revised: July 22, 2024
Accepted: July 23, 2024
Published: August 5, 2024

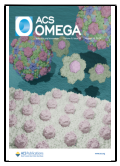

Scheme 1. Schematic Illustration of SCTP Cryogel as Antibacterial Photodynamic Wound Dressing

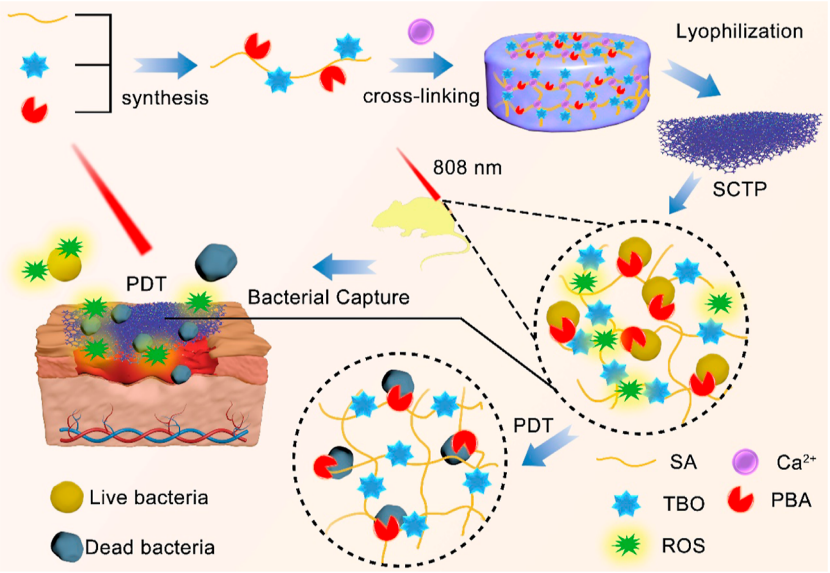

Surface modification of nanoagents with phenylboronic acid (PBA) has been demonstrated to enhance targeted antibacterial therapies by forming dynamic boronic ester bonds with diol groups on bacterial cell walls.[31−35] This approach has been effectively utilized in various nanoagents, including silver nanoparticles, to achieve targeted PTT and PDT against bacteria.[36,37] By exploiting the bacteria-targeting capability of PBA, these modified nanoagents offer improved therapeutic efficacy while minimizing adverse effects. Inspired by this strategy, surface immobilization of cryogels with PBA holds promise for developing photodynamic cryogels with enhanced antibacterial efficacy for anti-infective treatments.

In this investigation, with the activation of EDC and NHS, the carboxyl groups of SA can form an amide covalent bond with the amino groups in 3-aminophenylboronic acid (PBA) and the photosensitizer toluidine blue O (TBO) to produce SA@TBO@PBA molecules.[38,39] These molecules were cross-linked using Ca(II) ions to form SA@Ca(II)@TBO@PBA (SCTP) hydrogel, which was subsequently freeze-dried to create antibacterial SCTP cryogel dressings (Scheme 1). Thanks to its inherent high porosity, the SCTP cryogel exhibited excellent absorption of blood exudate, making it suitable for use as a wound dressing. Both in vitro and in vivo experiments confirmed the ability of the SCTP cryogel to rapidly stop bleeding when applied as a wound dressing. TBO, a commonly used cationic photosensitizer, has intrinsic toxicity and limited antibacterial efficacy. However, by covalently attaching TBO molecules to SA, its toxicity was significantly reduced. The formation of boronic ester bonds between PBA and diol groups on the bacterial cell surface allowed for the specific immobilization of *Staphylococcus aureus* (*S. aureus*) and *Escherichia coli* (*E. coli*) by the SCTP cryogel, facilitating TBO-mediated photodynamic inactivation of bacteria. Consequently, in vitro antibacterial assays demonstrated the enhanced efficiency of PDT upon laser irradiation. These promising findings suggest that nonantibiotic cryogel wound dressings, such as SCTP cryogel, have the potential for use in the treatment of skin wounds in the future.

2. MATERIAL AND METHODS

2.1. Preparation of SCTP Cryogel. Aqueous solutions of SA, SA@TBO, or SA@TBO@PBA (2%) were poured into a 6-well plate to serve as molds and refrigerated at 4 °C to eliminate bubbles. After lyophilization, porous skeletons were formed. These skeletons were then cross-linked with a 500 mM $CaCl_2$ solution. Finally, the cryogels were obtained through a second lyophilization process.

2.2. Singlet Oxygen Generation of STP Cryogel. DPBF was employed as a probe to detect the generation of $^1O_2$. SC, SCT, or SCTP cryogels were placed at the bottom of a cuvette. Then, 2 mL of a DPBF solution in acetonitrile (0.04 mM) was added. The mixtures were exposed to 630 nm laser light at 50 mW/cm^2 for 1 min. The absorption spectrum of the samples was recorded every 10 s using a UV−vis spectrophotometer. For comparison, the absorbances of the cryogels without irradiation were also measured.

2.3. Bacteria Culture. Gram-positive bacteria *S. aureus* (ATCC 25923) and Gram-negative bacteria *E. coli* (ATCC 25922) were kindly provided by Guangzhou Institute of Microbiology. The single colony of bacteria was suspended in LB medium and then incubated overnight at 37 °C under 220 rpm shaking. After centrifugation, logarithmic growth bacteria were obtained and resuspended in fresh LB medium.

2.4. In Vitro Antibacterial Assays. The antibacterial efficacy of the cryogels was evaluated in vitro using *S. aureus* and *E. coli*. Prior to the experiment, both the devices and cryogels underwent preirradiation with a ultraviolet lamp for 30 min. Subsequently, the cryogels (SC, SCT, or SCTP) were exposed to bacterial suspensions (500 μL, with a concentration of 10^6 CFU/mL) and incubated in the dark for 3 h in separate wells of a 48-well plate. The samples were then divided into groups for light treatment, while others remained in darkness. The light treatment groups were subjected to 630 nm laser light (at 50 mW/cm^2) for 30 min. Finally, the antibacterial effectiveness of the cryogels was assessed by counting the number of bacterial colonies on agar plates after incubating them at 37 °C for 12 h, using the following formula

$$\text{antibacterial rate } (\%) = (N_C - N_S)/N_C \times 100\% \quad (1)$$

https://doi.org/10.1021/acsomega.4c04744
ACS Omega 2024, 9, 35845−35852

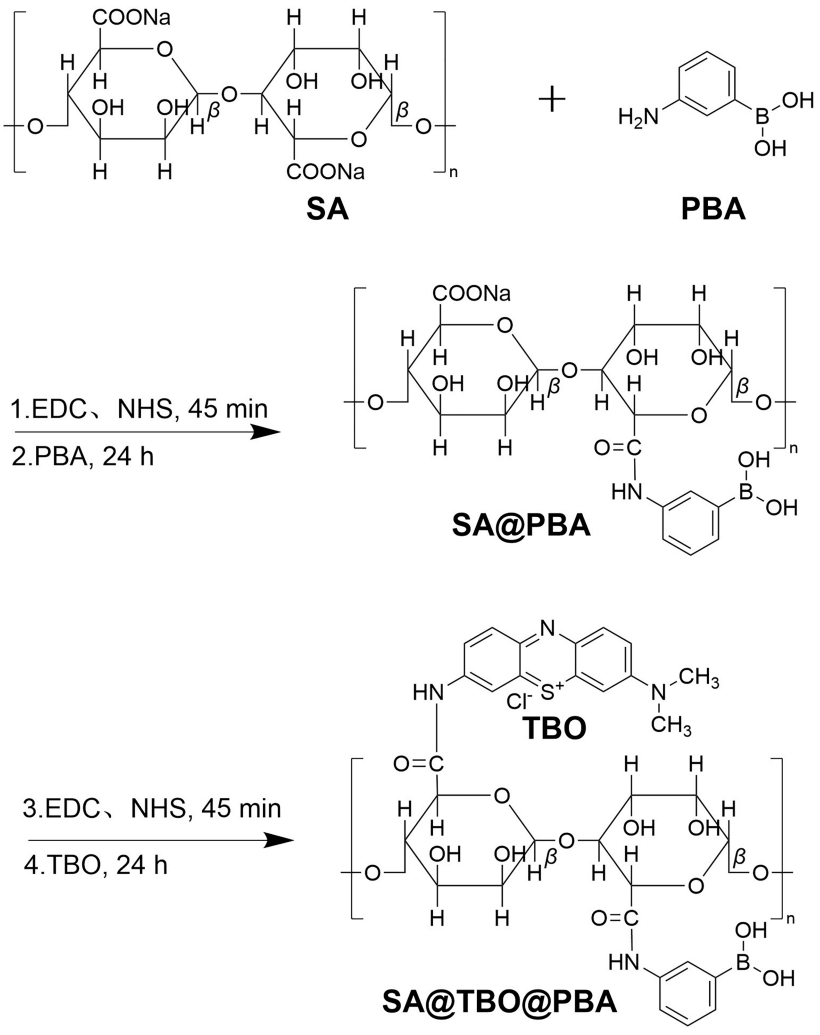

Figure 1. Synthesis of SA@TBO@PBA molecules.

where N_C is the number of colonies incubated with DI water (deionized water), and N_S stands for the number of colonies incubated with the cryogels.

2.5. Hemolysis Assays of STP Cryogel. 1 mL of blood from Balb/c mice was combined with 9 mL of 0.9% NaCl solution and then centrifuged at 750 rpm for 10 min. After discarding the supernatant, the remaining red blood cells (RBCs) were washed several times with a significant volume of 0.9% NaCl until the supernatant appeared colorless. Finally, the RBCs were diluted with 0.9% NaCl to achieve a concentration of 4% (volume concentration).

To begin, the cryogels were pulverized into fine powder for ease of handling in subsequent steps. This was done for all types of cryogels: SC, SCT, and SCTP. Next, suspensions of the powdered cryogels at different concentrations were prepared and mixed with a solution containing RBCs. After allowing the mixtures to sit at 37 °C for 2 h, they were centrifuged at 5000 rpm for 5 min. The resulting supernatant, containing released hemoglobin, was left at room temperature for 30 min to ensure complete oxidation of hemoglobin to oxyhemoglobin. For comparison: RBCs treated with Triton X-100 and RBCs treated with 0.9% NaCl were employed as positive and negative control groups, respectively. Finally, the absorbance at 540 nm was measured using a microplate reader, and the hemolysis rate (HR) was determined using the following formula

$$\mathrm{HR}(\%) = (A_s - A_n)/(A_p - A_n) \times 100\% \quad (2)$$

where A_s is the absorbance of RBCs incubated with cryogels, A_N reflects the absorbance of RBCs incubated with 0.9% NaCl, and A_P stands for the absorbance of RBCs incubated with DI water.

2.6. Animal. All animal experiments were approved by the Animal Ethics Committee of Guangdong Medical University (GDY2402002) and carried out in accordance with the National Research Council's Guide for the Care and Use of Laboratory Animals. The standardized and specific-pathogen-free (SPF) grade female Balb/c mice (6−8 weeks, Guangdong Provincial Animal Center) were raised in SPF animal room at the animal center of Guangdong Medical University and were acclimatized for 1 week before animal assays. Every effort was made to minimize animal suffering and reduce the number of animals used in the experiment.

2.7. Hemostatic Assays of SCTP Cryogel. The hemostatic capabilities of the cryogels were examined through a mouse-tail cutting experiment, employing gauze, SC, SCT, and SCTP cryogels. Twelve Balb/c mice were randomly distributed across the four groups. A section equivalent to 30% of each mouse's tail length was severed, and the resulting wounds were promptly treated with one of the designated materials: gauze, SC, SCT, or SCTP cryogels. Subsequently, the efficacy of each treatment was

https://doi.org/10.1021/acsomega.4c04744
ACS Omega 2024, 9, 35845−35852

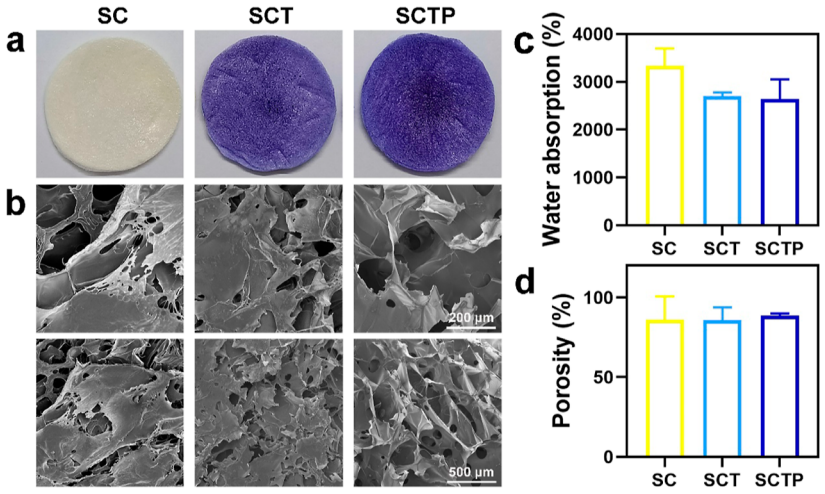

Figure 2. (a) The photographs, (b) morphologies, (c) water absorption rates and (d) porosity rates of SC, SCT and SCTP cryogels. Scale bars: 200 and 500 μm.

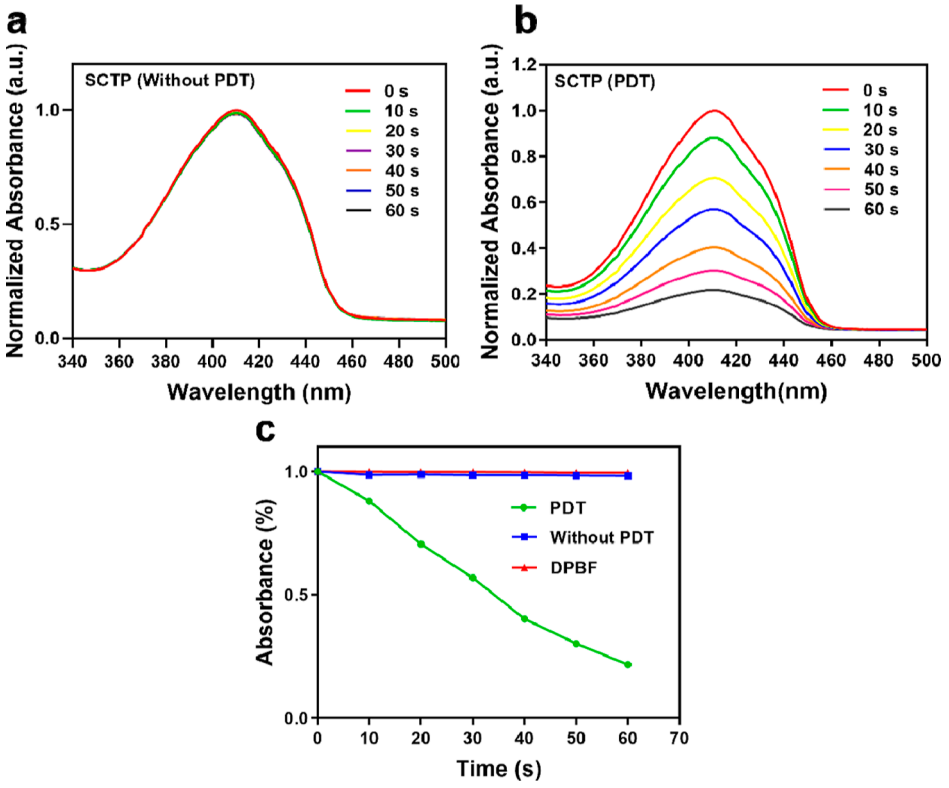

Figure 3. (a,b) UV−vis absorption spectra of DPBF treated with SCTP cryogel in the presence or absence of 630 nm laser light. (c) Absorbance of DPBF at the 410 nm.

evaluated by comparing the quantity of blood loss and the duration required for hemostasis to be achieved.

2.8. Statistical Analysis. All the results are reported as mean ± SD. The differences among groups were determined using one-way ANOVA analysis (*P < 0.05, **P < 0.01, ***P < 0.001).

3. RESULTS AND DISCUSSION

3.1. Generation and Characterization of SCTP Cryogel. To verify the successful immobilization of TBO and PBA onto SA, UV−vis spectroscopy was employed (Figures 1 and S1), which indicated grafting rates of 2.0% for TBO and 5.5% for PBA. Compared with SA, the UV−vis spectra of STP has the characteristic absorption peaks of TBO and PBA. Therefore, the TBO and PBA have successfully modified SA. The SCTP cryogel was then produced by lyophilizing the Ca(II)-cross-linked SCTP hydrogel (Scheme 1). The purple color of the SCTP cryogel, as shown in Figure 2a, confirmed the successful synthesis of the SA@TBO@PBA molecules. SEM was used to analyze the morphology of the cryogels. The images displayed a lamellar and porous structure, essential for absorbing blood exudates during hemostasis and capturing bacteria (Figure 2b). The cryogels' water absorption ability and porosity were also evaluated, demonstrating that the SCTP cryogel achieved a high water absorption capacity of 2642.5% and a porosity of 88.6%,

https://doi.org/10.1021/acsomega.4c04744
ACS Omega 2024, 9, 35845−35852

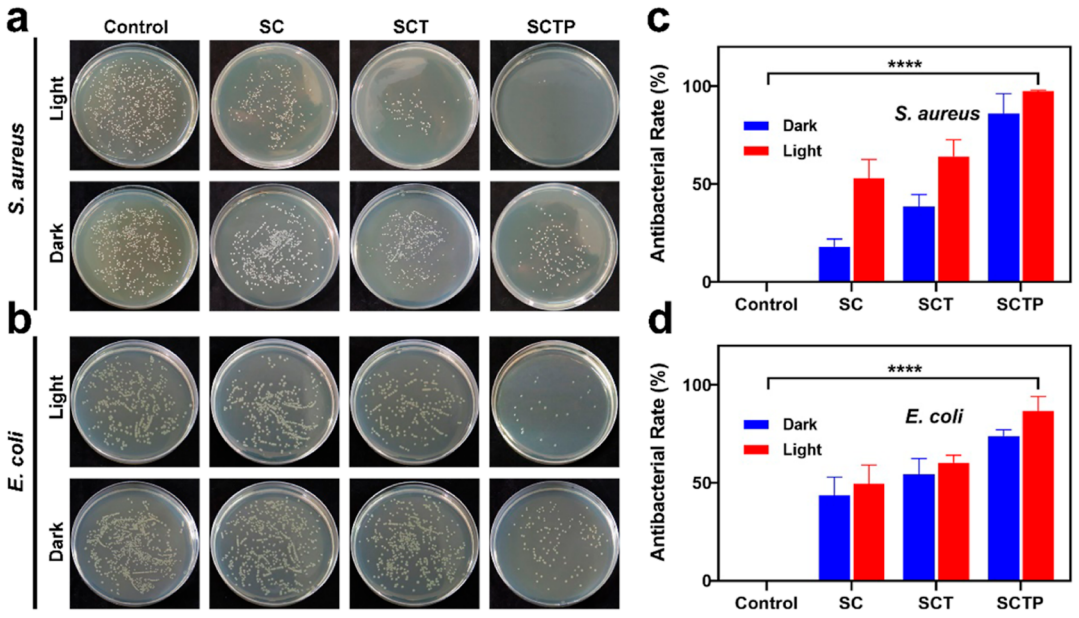

Figure 4. Representative plate photographs of (a) *S. aureus* and (b) *E. coli* colonies after different treatments. The corresponding antibacterial rates of (c) *S. aureus* and (d) *E. coli* after different treatments obtained by the plate counting method (P values were calculated by two-way ANOVA test, $n = 3$, $^{****}P < 0.001$, $^{***}P < 0.001$, $^{**}P < 0.01$, or $^{*}P < 0.05$).

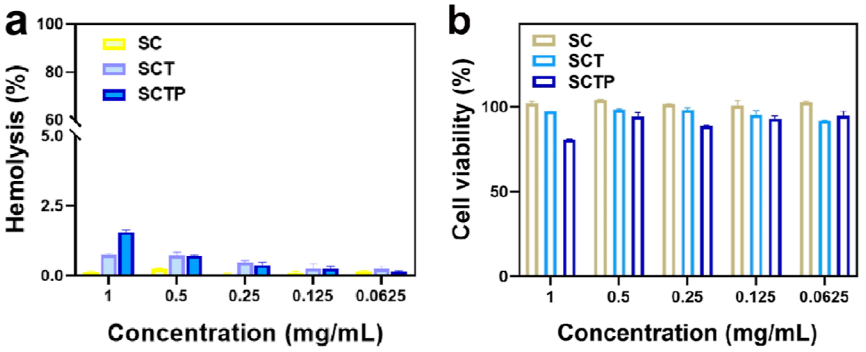

Figure 5. (a) Relative hemolysis ratios and (b) cell viability of L929 cells treated with SC, SCT and SCTP cryogels at different concentrations.

which are beneficial for their hemostatic function (Figure 2c,d). These properties confirm that all prepared cryogels exhibit excellent water absorption capacity, necessary for effective wound dressings.[40]

In addition, we evaluated the dynamic swelling of SCTP cryogel. The results were shown in Figure S2. The SCTP cryogel showed rapid swelling within 5 min, and then reached swelling equilibrium after 30 min with the swelling rate of 3053.3%. The result showed that the SCTP cryogel could swell to equilibrium within 30 min, and had a high swelling rate.

Subsequently, we evaluated the stability of SCTP cryogel under different temperature conditions (37, 45 and 60 °C). The results are shown in Figure S3. As can be seen from the photos, the color of the SCTP cryogels did not change after 7 days at different temperatures (37, 45 and 60 °C), and the shape remained intact without chapping. In addition, as can be seen from Figure S4, the cryogels had little change in weight over 7 days except for a slight loss of water. It indicates that the SCTP cryogel is stable below 60 °C and can be stored for a certain time.

Because $^1O_2$ is crucial for killing bacteria in PDT, it is important to assess how much $^1O_2$ a material can produce. In this study, we used a method called the DPBF assay to measure $^1O_2$ production by the SCTP cryogel (Figure 3). DPBF reacts with $^1O_2$ to form a nonabsorbing compound, and we measured the decrease in absorption at 410 nm to quantify $^1O_2$ production.[41] When the SCTP cryogel was exposed to 630 nm laser light, there was a significant reduction in DPBF absorption compared to control samples (Figure 3a,b). Furthermore, by adjusting the duration of laser irradiation, we could control the amount of $^1O_2$ produced (Figure 3c), demonstrating the potential of the SCTP cryogel for use in antibacterial photodynamic therapy (aPDT).

3.2. In Vitro Bacterial Capture and Antibacterial Activities of SCTP Cryogel. PBA has gained attention for its ability to interact with bacterial surfaces, making it useful in bacterial detection and anti-infective therapy.[37] In our study, we incorporated PBA into the SCTP cryogel to capture bacteria through covalent binding. This design aimed to enhance the efficiency of photodynamic bacterial inactivation by reducing the distance between bacteria and the $^1O_2$ generated by TBO under 630 nm laser irradiation. Since wound dressings are applied directly to wounds, it is crucial to ensure effective antibacterial activity against wound infections. To evaluate its antibacterial abilities against *S. aureus* and *E. coli*, we conducted experiments using the plate counting method, with or without 630 nm laser irradiation (Figure 4). We observed no significant

https://doi.org/10.1021/acsomega.4c04744
ACS Omega 2024, 9, 35845−35852

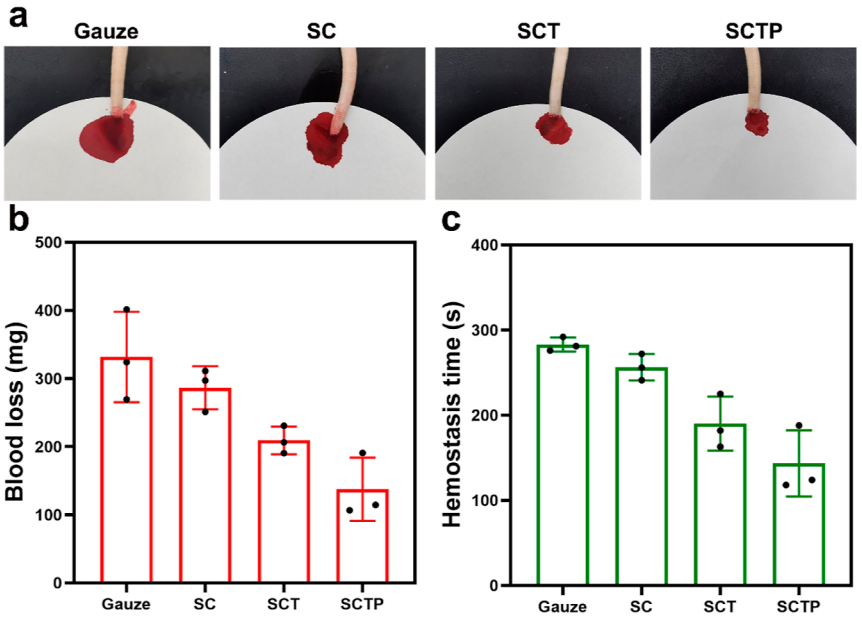

Figure 6. (a) Blood loss, (b) hemostasis time and (c) photographs of the hemostasis on the truncated mice-tail model by using gauze, SC, SCT and SCTP cryogels.

difference in bacterial viability when treated with the SC cryogel with or without laser irradiation. Next, we tested the SCT and SCTP cryogels without laser irradiation (Figure 4a,b). The SCT cryogel showed limited antibacterial activity (38.6% for *S. aureus* and 54.4% for *E. coli*), likely due to the dark toxicity of TBO. However, the SCTP cryogel, with PBA's bacterial targeting effect, showed improved toxicities against bacteria (86.2% for *S. aureus* and 73.9% for *E. coli*). Finally, we assessed the therapeutic efficiency of aPDT by exposing the SCT and SCTP cryogels to bacteria under 630 nm laser irradiation. While the SCT cryogel showed moderate antibacterial rates (64.1% for *S. aureus* and 60.3% for *E. coli*), PBA modification significantly enhanced the aPDT efficiency of the SCTP cryogel (97.5% for *S. aureus* and 86.6% for *E. coli*) (Figure 4c,d). The enhanced antibacterial effect observed with SCTP cryogels highlights the importance of PBA-mediated bacterial targeting, resulting in substantially higher antibacterial rates against both *S. aureus* and *E. coli*. In summary, our findings underscore the significant role of PBA in enhancing the aPDT efficiency of the SCTP cryogel, making it a promising candidate for combating bacterial infections in wounds.

3.3. In Vitro Biosafety of SCTP Cryogel. Hemolysis and Cell Counting Kit-8 (CCK-8) assays were conducted to evaluate the biocompatibility of the cryogels, including SC, SCT, and SCTP cryogels (Figure 5). In the hemolytic test, mouse RBCs were exposed to different concentrations of SC, SCT, and SCTP cryogels, while positive and negative controls were Triton X-100 and 0.9% NaCl, respectively. The positive control showed complete RBC rupture, indicating hemolysis, while no significant hemolysis was observed in the negative control or any cryogel group, even at the highest concentration (1 mg/mL). Notably, the HR of the SCTP cryogel (1.6%) remained below the permissible limit (5%) at the highest concentration (Figure 5a). Moreover, CCK-8 assays on the mouse fibroblast cells (L929 cells) revealed minimal cytotoxicity for all cryogel types, even at 1 mg/mL (Figure 5b). Overall, these results highlight the excellent biosafety of the SCTP cryogel for potential *in vivo* applications.

3.4. Hemostatic Characterization of SCTP Cryogel. To prevent excessive post-traumatic bleeding, hemostasis is an essential evaluation index for wound dressings.[40] To evaluate the SCTP cryogel's ability to stop bleeding effectively, Balb/c mice were employed as an animal model by cutting down part of their tails to evaluate the hemostatic property of the SCTP cryogel (Figure 6a). We compared blood loss and hemostatic time using various materials: gauze, SC, SCT and SCTP cryogels. The results showed that gauze application resulted in substantial blood loss and prolonged bleeding for approximately 5 min. Conversely, the use of SC and SCT cryogels significantly reduced blood loss and the time needed for hemostasis. Notably, the SCTP cryogel exhibited superior hemostatic properties, reducing blood loss and the time for hemostasis by 58.6 and 49.4%, respectively, compared to gauze(Figure 6b,c). The above findings indicate that SCTP cryogel has the excellent hemostatic ability in the tail amputation hemorrhage models which could attribute to the strong adhesion between the PBA of SCTP cryogel and the surface of the wound. This adhesion is due to the combination of PBA and sugar-based compounds present on biological cell membranes. These findings underscore the potential of the SCTP cryogel as an effective wound dressing for promoting hemostasis.

4. CONCLUSION

To summarize, we've created a new type of wound dressing called the SCTP cryogel. It provides quick clotting and better aPDT without antibiotics. This cryogel is made by attaching the photosensitizer TBO and PBA to SA chemically. With the help of PBA's bacteria-targeting effect, our tests in the lab showed a notable improvement in treatment effectiveness under 630 nm laser light. Also, the cryogel has high absorbency, which helps in absorbing blood and promoting fast clotting. In vivo assays confirmed its effectiveness in stopping bleeding, making it a promising option for clinical trials as a wound dressing.

https://doi.org/10.1021/acsomega.4c04744
ACS Omega 2024, 9, 35845−35852

■ ASSOCIATED CONTENT

Data Availability Statement

The raw/processed data required to reproduce these findings cannot be shared at this time as the data also forms part of an ongoing study.

Supporting Information

The Supporting Information is available free of charge at https://pubs.acs.org/doi/10.1021/acsomega.4c04744.

UV−vis absorption spectra of SA, PBA, TBO, SA@TBO and SA@TBO@PBA molecules (Figure S1); the swelling rate of SCTP cryogel (Figure S2); photos of the SCTP cryogels stored at different temperatures (37, 45 and 60 °C) for different times (1, 2, 3, 4, 5, 6 and 7d) (Figure S3); weight changes of the SCTP cryogels after storage at different temperatures (37, 45 and 60 °C) for different times (1, 2, 3, 4, 5, 6 and 7d) (Figure S4) (PDF)

■ AUTHOR INFORMATION

Corresponding Authors

Yang Zhang − *Guangdong Dongguan Quality Supervision Testing Center, Dongguan 523000, China*; Email: zyxx2010@163.com

Ning Guo − *Dongguan Children's Hospital; School of Pharmacy, Guangdong Medical University, Dongguan 523000, China*; orcid.org/0000-0001-5305-5636; Email: guoning19890501@163.com

Authors

Xiaocheng Lin − *Dongguan Children's Hospital; School of Pharmacy, Guangdong Medical University, Dongguan 523000, China*

Jia Chen − *Dongguan Children's Hospital; School of Pharmacy, Guangdong Medical University, Dongguan 523000, China*

Yu Xia − *Dongguan Children's Hospital; School of Pharmacy, Guangdong Medical University, Dongguan 523000, China*

Yan Chen − *Dongguan Children's Hospital; School of Pharmacy, Guangdong Medical University, Dongguan 523000, China*

Huixuan Gan − *Dongguan Children's Hospital; School of Pharmacy, Guangdong Medical University, Dongguan 523000, China*

Zhongjia Liu − *Dongguan Children's Hospital; School of Pharmacy, Guangdong Medical University, Dongguan 523000, China*

Quanxin Wu − *Dongguan Children's Hospital; School of Pharmacy, Guangdong Medical University, Dongguan 523000, China*

Complete contact information is available at: https://pubs.acs.org/10.1021/acsomega.4c04744

Author Contributions

[§]X.L., J.C. and Y.X. contributed equally to this work. **Xiaocheng Lin:** Investigation, Writing−original draft. **Jia Chen:** Investigation, Data curation. **Yu Xia:** Investigation. **Yan Chen:** Investigation. **Huixuan Gan:** Investigation. **Zhongjia Liu:** Investigation. **Quanxin Wu:** Investigation. **Yang Zhang:** Investigation, Writing−review and editing. **Ning Guo:** Funding acquisition, Writing−review and editing.

Notes

The authors declare no competing financial interest.

■ ACKNOWLEDGMENTS

This research was financially supported by Innovation Program of Zhanjiang (2020LHJH005), Dongguan Science and Technology of Social Development Program (20221800905352), Guangdong Basic and Applied Basic Research Foundation (2023A1515140078) and Medical Research Foundation of Guangdong (A2024466).

■ REFERENCES

(1) Gaston, E.; Fraser, J.; Xu, Z.; Ta, H. Nano- and micro-materials in the treatment of internal bleeding and uncontrolled hemorrhage. *Nanomed. Nanotechnol.* **2018**, *14*, 507−519.

(2) Zhuo, S.; Liang, Y.; Wu, Z.; Zhao, X.; Han, Y.; Guo, B. Supramolecular hydrogels for wound repair and hemostasis. *Mater. Horiz.* **2024**, *11*, 37−101.

(3) Vloemans, A. F. P. M.; Soesman, A. M.; Kreis, R. W.; Middelkoop, E. A newly developed hydrofibre dressing, in the treatment of partial-thickness burns. *Burns* **2001**, *27*, 167−173.

(4) Bužarovska, A.; Selaru, A.; Serban, M.; Pircalabioru, G. G.; Costache, M.; Cocca, M.; Gentile, G.; Avérous, L.; Dinescu, S. Biobased multiphase foams with ZnO for wound dressing applications. *J. Mater. Sci.* **2023**, *58*, 17594−17609.

(5) Huang, R.; Hua, Z.; Li, L.; Zhou, Y.; Xu, Y.; Zhang, T. Effect of hydrocolloid dressings in the management of different grades of pressure wound ulcers in critically ill adult subjects: A meta-analysis. *Int. Wound J.* **2023**, *20*, 3981−3989.

(6) Akin, B.; Ozmen, M. M. Antimicrobial cryogel dressings towards effective wound healing. *Prog. Biomater.* **2022**, *11*, 331−346.

(7) Zhang, Y.; Wang, Y.; Chen, L.; Zheng, J.; Fan, X.; Xu, X.; Zhou, G.; Ullah, N.; Feng, X. An injectable antibacterial chitosan-based cryogel with high absorbency and rapid shape recovery for noncompressible hemorrhage and wound healing. *Biomaterials* **2022**, *285*, 121546.

(8) Andrabi, S. M.; Kumar, A. A kaolin/calcium incorporated shape memory and antimicrobial chitosan-dextran based cryogel as an efficient haemostatic dressing for uncontrolled hemorrhagic wounds. *Biomater. Adv.* **2023**, *150*, 213424.

(9) Wang, M.; Hu, J.; Ou, Y.; He, X.; Wang, Y.; Zou, C.; Jiang, Y.; Luo, F.; Lu, D.; Li, Z.; Li, J.; Tan, H. Shape-recoverable hyaluronic acid-waterborne polyurethane hybrid cryogel accelerates hemostasis and wound healing. *ACS Appl. Mater. Interfaces* **2022**, *14*, 17093−17108.

(10) Cao, S.; Bi, Z.; Li, Q.; Zhang, S.; Singh, M.; Chen, J. Shape memory and antibacterial chitosan-based cryogel with hemostasis and skin wound repair. *Carbohydr. Polym.* **2023**, *305*, 120545.

(11) Shan, L.; Gao, Y.; Zhang, Y.; Yu, W.; Yang, Y.; Shen, S.; Zhang, S.; Zhu, L.; Xu, L.; Tian, B.; Yun, J. Fabrication and use of alginate-based cryogel delivery beads loaded with urea and phosphates as potential carriers for bioremediation. *Ind. Eng. Chem. Res.* **2016**, *55*, 7655−7660.

(12) Bauleth-Ramos, T.; Shih, T.; Shahbazi, M.; Najibi, A. J.; Mao, A. S.; Liu, D.; Granja, P.; Santos, H. A.; Sarmento, B.; Mooney, D. J. Acetalated dextran nanoparticles loaded into an injectable alginate cryogel for combined chemotherapy and cancer vaccination. *Adv. Funct. Mater.* **2019**, *29*, 1903686.

(13) Tripathi, A.; Kumar, A. Multi-featured macroporous agarose-alginate cryogel: synthesis and characterization for bioengineering applications. *Macromol. Biosci.* **2011**, *11*, 22−35.

(14) Sood, A.; Dev, A.; Das, S. S.; Kim, H. J.; Kumar, A.; Thakur, V. K.; Han, S. S. Curcumin-loaded alginate hydrogels for cancer therapy and wound healing applications: A review. *Int. J. Biol. Macromol.* **2023**, *232*, 123283.

(15) Rosselle, L.; Cantelmo, A. R.; Barras, A.; Skandrani, N.; Pastore, M.; Aydin, D.; Chambre, L.; Sanyal, R.; Sanyal, A.; Boukherroub, R.; Szunerits, S. An 'on-demand' photothermal antibiotic release cryogel patch: evaluation of efficacy on an ex vivo model for skin wound infection. *Biomater. Sci.* **2020**, *8*, 5911−5919.

(16) Yavuz, B.; Kondolot Solak, E.; Oktar, C. Preparation of biocompatible microsphere-cryogel composite system and controlled release of mupirocin. *Int. J. Polym. Mater. Polym.* **2024**, *73*, 354−361.

(17) Gottesdiener, L. S.; Satlin, M. J. Global impact of antibacterial resistance in patients with hematologic malignancies and hematopoietic cell transplant recipients. *Transplant Infect. Dis.* **2023**, *25*, No. e14169.
(18) Li, T.; Wang, Z.; Guo, J.; de la Fuente-Nunez, C.; Wang, J.; Han, B.; Tao, H.; Liu, J.; Wang, X. Bacterial resistance to antibacterial agents: Mechanisms, control strategies, and implications for global health. *Sci. Total Environ.* **2023**, *860*, 160461.
(19) Neill, J. O. *Tackling drug-resistant infections globally: Final report and recommendations*, 2016. http://amr-review.org/sites/default/files/160525_Final%20paper_with%20cover.pdf.
(20) Lin, X.; Duan, Y.; Lan, Q.; Xu, Y.; Xia, Y.; Huang, Z.; Song, L.; Zhang, Y.; Guo, N. Alginate-based cryogels for combined chemo/photothermal antibacterial therapy and rapid hemostasis. *ACS Omega* **2023**, *8*, 4889−4898.
(21) Xu, Y.; Cai, Y.; Xia, Y.; Wu, Q.; Li, M.; Guo, N.; Tu, Y.; Yang, B.; Liu, Y. Photothermal nanoagent for anti-inflammation through macrophage repolarization following antibacterial therapy. *Eur. Polym. J.* **2023**, *186*, 111840.
(22) Wang, R.; Liu, Q.; Gao, A.; Tang, N.; Zhang, Q.; Zhang, A.; Cui, D. Recent developments of sonodynamic therapy in antibacterial application. *Nanoscale* **2022**, *14*, 12999−13017.
(23) Roy, J.; Pandey, V.; Gupta, I.; Shekhar, H. Antibacterial sonodynamic therapy: Current status and future perspectives. *ACS Biomater. Sci. Eng.* **2021**, *7*, 5326−5338.
(24) Guo, N.; Xia, Y.; Duan, Y.; Wu, Q.; Xiao, L.; Shi, Y.; Yang, B.; Liu, Y. Self-enhanced photothermal-chemodynamic antibacterial agents for synergistic anti-infective therapy. *Chin. Chem. Lett.* **2023**, *34*, 107542.
(25) Zhao, S.; Xia, Y.; Lan, Q.; Wu, Q.; Feng, X.; Liu, Y. pH-responsive nanogel for photothemal-enhanced chemodynamic antibacterial therapy. *ACS Appl. Nano Mater.* **2023**, *6*, 8643−8654.
(26) Xu, Y.; Zhou, W.; Xiao, L.; Lan, Q.; Li, M.; Liu, Y.; Song, L.; Li, L. Bacitracin-engineered BSA/ICG nanocomplex with enhanced photothermal and photodynamic antibacterial activity. *ACS Omega* **2022**, *7*, 33821−33829.
(27) Badran, Z.; Rahman, B.; De Bonfils, P.; Nun, P.; Coeffard, V.; Verron, E. Antibacterial nanophotosensitizers in photodynamic therapy: An update. *Drug Discovery Today* **2023**, *28*, 103493.
(28) Wang, C.; Lin, Y.; Huang, J.; Song, H.; Zhang, Y.; Zhang, Y.; Xu, M.; Liu, J. Pseudomonas aeruginosa targeting cascade photodynamic nanoassemblies for efficient antibacterial and anti-inflammatory therapy. *Nano Today* **2023**, *51*, 101892.
(29) Hu, X.; Zhang, H.; Wang, Y.; Shiu, B.; Lin, J.; Zhang, S.; Lou, C.; Li, T. Synergistic antibacterial strategy based on photodynamic therapy: Progress and perspectives. *Chem. Eng. J.* **2022**, *450*, 138129.
(30) Thomas-Moore, B. A.; del Valle, C. A.; Field, R. A.; Marín, M. J. Recent advances in nanoparticle-based targeting tactics for antibacterial photodynamic therapy. *Photochem. Photobiol. Sci.* **2022**, *21*, 1111−1131.
(31) Liu, J.; Zheng, Z.; Luo, J.; Wang, P.; Lu, G.; Pan, J. Engineered reversible adhesive biofoams for accelerated dermal wound healing: Intriguing multi-covalent phenylboronic acid/cis-diol interaction. *Colloids Surf., B* **2023**, *221*, 112987.
(32) Gong, H.; Liu, W.; Carlquist, M.; Ye, L. Boronic acid modified polymer nanoparticles for enhanced bacterial deactivation. *ChemBioChem* **2019**, *20*, 2991−2995.
(33) Beyranvand, S.; Pourghobadi, Z.; Sattari, S.; Soleymani, K.; Donskyi, I.; Gharabaghi, M.; Unger, W. E. S.; Farjanikish, G.; Nayebzadeh, H.; Adeli, M. Boronic acid functionalized graphene platforms for diabetic wound healing. *Carbon* **2020**, *158*, 327−336.
(34) Jayeoye, T. J.; Olatunde, O. O.; Benjakul, S.; Rujiralai, T. Synthesis and characterization of novel poly(3-aminophenyl boronic acid-co-vinyl alcohol) nanocomposite polymer stabilized silver nanoparticles with antibacterial and antioxidant applications. *Colloids Surf., B* **2020**, *193*, 111112.
(35) Chen, M.; Zhang, J.; Qi, J.; Dong, R.; Liu, H.; Wu, D.; Shao, H.; Jiang, X. Boronic acid-decorated multivariate photosensitive metal−organic frameworks for combating multi-drug-resistant bacteria. *ACS Nano* **2022**, *16*, 7732−7744.
(36) Wang, H.; You, W.; Wu, B.; Nie, X.; Xia, L.; Wang, C.; You, Y. Phenylboronic acid-functionalized silver nanoparticles for highly efficient and selective bacterial killing. *J. Mater. Chem. B* **2022**, *10*, 2844−2852.
(37) Liu, Y.; Lan, Q.; Liu, J.; Shi, Y.; Wu, Q.; Wang, Q.; Yang, S.; Cheng, F. Phenylboronic acid-functionalized BSA@CuS@PpIX nanoparticles for enhanced antibacterial photodynamic/photothermal therapy. *J. Drug Delivery Sci. Technol.* **2023**, *88*, 104965.
(38) Ding, C.; Zhang, F.; Gao, Y.; Li, Y.; Cheng, D.; Wang, J.; Mao, L. Antibacterial photodynamic treatment of porphyromonas gingivalis with toluidine blue O and a nonlaser red light source enhanced by dihydroartemisinin. *Photochem. Photobiol.* **2021**, *97*, 377−384.
(39) Misba, L.; Abdulrahman, H.; Khan, A. U. Photodynamic efficacy of toluidine blue O against mono species and dual species bacterial biofilm. *Photodiagn. Photodyn.* **2019**, *26*, 383−388.
(40) Chen, J.; Xia, Y.; Lan, Q.; Hu, M.; Xu, Y.; Wu, Q.; Liu, X.; Liu, Y. Alginate based photothermal cryogels boost ferrous-supply for enhanced antibacterial chemodynamic therapy and accelerated wound healing. *Int. J. Biol. Macromol.* **2023**, *232*, 123473.
(41) Cheng, F.; Huang, Q.; Li, Y.; Huang, Z.; Wu, Q.; Wang, W.; Liu, Y.; Wang, G. Combined chemo and photo therapy of programmable prodrug carriers to overcome delivery barriers against nasopharyngeal carcinoma. *Biomater. Adv.* **2023**, *151*, 213451.

https://doi.org/10.1021/acsomega.4c04744
ACS Omega 2024, 9, 35845−35852